

Differences in endplate deformation of the adjacent and augmented vertebra following cement augmentation

Paul A. Hulme · S. K. Boyd · P. F. Heini ·
S. J. Ferguson

Received: 26 September 2007 / Revised: 26 January 2009 / Accepted: 4 February 2009
© Springer-Verlag 2009

Abstract Vertebral cement augmentation can restore the stiffness and strength of a fractured vertebra and relieve chronic pain. Previous finite element analysis, biomechanical tests and clinical studies have indirectly associated new adjacent vertebral fractures following augmentation to altered loading. The aim of this repeated measures in situ biomechanical study was to determine the changes in the adjacent and augmented endplate deformation following cement augmentation of human cadaveric functional spine units (FSU) using micro-computed tomography (micro-CT). The surrounding soft tissue and posterior elements of 22 cadaveric human FSU were removed. FSU were assigned to two groups, control ($n = 8$) (loaded on day 1 and day 2) and augmented ($n = 14$) (loaded on day 1, augmented 20% cement fill, and loaded on day 2). The augmented group was further subdivided into a prophylactic augmentation group ($n = 9$), and vertebrae which spontaneously fractured during loading on day 1 ($n = 5$). The FSU were axially loaded (200, 1,000, 1,500–2,000 N) within a custom made radiolucent, saline filled loading device. At each loading step, FSUs were scanned using the micro-CT. Endplate heights were determined using custom software. No significant increase in endplate deformation

following cement augmentation was noted for the adjacent endplate ($P > 0.05$). The deformation of the augmented endplate was significantly reduced following cement augmentation for both the prophylactic and fracture group ($P < 0.05$, $P < 0.01$, respectively). Endplate deformation of the controls showed no statistically significant differences between loading on day 1 and day 2. A linear relationship was noted between the applied compressive load and endplate deflection ($R^2 = 0.58$). Evidence of significant endplate deformation differences between unaugmented and augmented FSU, while evident for the augmented endplate, was not present for the adjacent endplate. This non-invasive micro-CT method may also be useful to investigate endplate failure, and parameters that predict vertebral failure.

Keywords Cement augmentation · Vertebroplasty · Adjacent fractures · Micro-CT · Vertebral endplate

Introduction

Osteoporosis is estimated to afflict 200 million women worldwide [21]. A total of 700,000 vertebral fractures are reported in US each year, outnumbering fractures of the hip and ankle combined [6, 43, 48, 54]. Vertebral fractures may result in local pain about the fracture site, loss of height due to vertebral collapse, spinal instability and in many cases kyphotic deformity [45]. Chronic pain and kyphotic deformity may lead to depression, decreased appetite (leading to poor nutrition), decreased pulmonary function, impaired mobility and a reduction in the quality of life, the ultimate result being a significant increase in morbidity [7, 8, 10, 33]. The conventional treatments of medications, bracing and bed rest are not universally

P. A. Hulme (✉) · S. J. Ferguson
MEM Research Center, University of Bern, Stauffacherstrasse
78, 3014 Bern, Switzerland
e-mail: Paul.Hulme@MEMcenter.unibe.ch;
paul.hulme@zimmer.com

S. K. Boyd
Schulich School of Engineering, University of Calgary, Calgary,
AB, Canada

P. F. Heini
Department of Orthopaedic Surgery, Spine Service, Inselspital,
University of Bern, Bern, Switzerland

effective. Thus, interest has been fostered in percutaneous methods of fracture stabilization that reduce or eliminate pain allowing a return to normal activity in a short period of time.

Cement augmentation, through the injection of low viscosity liquid bone cement (usually polymethylmethacrylate, PMMA) into the damaged vertebral body, provides immediate pain relief [19], strengthens the affected vertebra and prevents further vertebral collapse [8]. The elastic modulus of PMMA cement is on average 12 times that of normal cancellous bone, thus a change in the mechanical behavior of the augmented and adjacent vertebra is plausible [2]. Finite element models and biomechanical tests of the augmented spinal segment have shown an increase in nucleus pulposus (NP) pressure, an increased deformation of the adjacent endplate [2, 24, 40], and a decrease in segmental strength [3, 40, 53]. Clinical studies have reported that the rate of vertebral fractures adjacent to a previously augmented vertebra occur sooner than non-adjacent fractures [47], the majority within 30 days [11, 49]. Although these findings may suggest that the risk of fracture is increased adjacent to an augmented vertebra, new fractures may be the result of the natural progression of osteoporosis. Indeed, some recent studies refute earlier findings, concluding that subsequent vertebral fractures are the result of excessive loading and not the augmentation process [1, 23, 51]. Therefore, due to the conflicting conclusions drawn by previous studies, the need still exists to determine the effect of cement augmentation on vertebral mechanics.

Axial overload is often associated with excessive endplate bulging, and fracture of the endplate or underlying trabecular bone [5]. Changes in loading, due to cement augmentation, will be evident in altered endplate behavior, which was measured using a non-invasive in situ, micro-computed tomography (micro-CT) method [18]. The specific aim of this repeated measures, in vitro, biomechanical study was to determine the effect of cement augmentation on endplate deformation of the adjacent and augmented vertebrae.

Methods

Specimen preparation

The surrounding soft tissue and posterior elements of 26 cadaveric human functional spine units (FSU) were removed (average 74.45 ± 4.25 years) from 13 spines. Vertebrae were grouped as follows: one T9–T10, three T11–T12, five T12–L1, eight L1–L2, three L2–L3, four L3–L4, and two L4–L5. Impressions were made of the cranial and caudal endplates in semi-cured bone cement

(Sulfix, Sulzer Orthopaedics Ltd). A jig ensured that the two end caps were parallel to each other. The molded end caps extended only to the cortical rim, thereby ensuring even loading without reinforcing the FSU. Small glass beads (>5 beads, ~ 1 mm diameter) were glued directly to the cortical shell just below each superior and inferior vertebral endplate and were used as fiducial markers for image registration (Fig. 1). Bone mineral density (BMD) was assessed using dual energy X-ray absorptiometry (DEXA) (Discovery C, Hologic, Bedford, MA) following the removal of the posterior vertebral elements. Anterior–posterior scans were performed. Posterior elements were removed prior to scanning, therefore, direct comparison with the World Health Organization definition of osteoporosis was not possible.

Specimen loading

The effect of cement augmentation on vertebral loading was evaluated using a custom compressive loading device in combination with a large gantry micro-CT (XtremeCT, Scanco Medical AG, Bassersdorf, Switzerland) which allowed for the non-invasive quantification of endplate deflection (Fig. 2) [18]. The specimen was bathed in physiological saline solution at all times. Load applied to the specimen and displacement of the loading platen were monitored using a miniature load cell (0–1,000 lbs, Sensotec, Model 31, $\pm 0.05\%$ FS repeatability) and a LVDT (0–5 mm, Burster model 8740-5005, $\pm 0.01\%$ FS repeatability), respectively.

Loads were chosen to represent rest (200 N), in vivo standing load (1,000 N, minimum load) [51], and light manual work (1,500–2,000 N, maximum load) [38]. At each load step, two scans were performed. Prior to the first scan a 45-min static loading phase was performed to minimize stress relaxation during scanning. The first scan

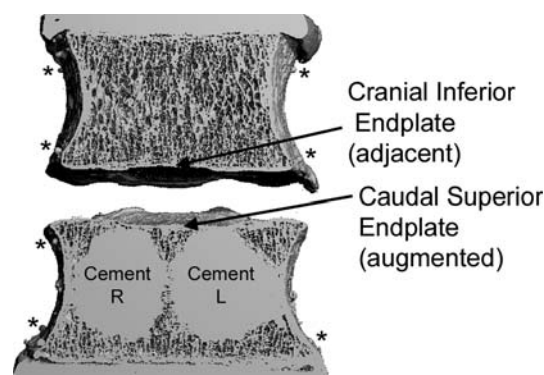


Fig. 1 Sagittal slice through an augmented FSU. Augmentation was performed bilaterally. Cement was evenly distributed between the two sides to fill 20% of the vertebral volume (asterisks indicate the position of a fiducial marker)

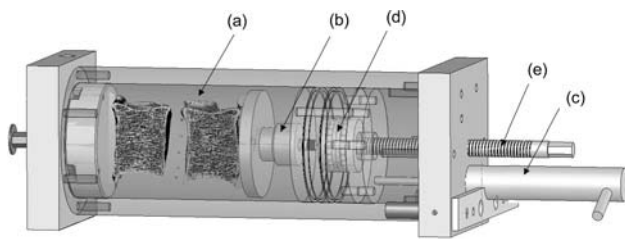


Fig. 2 Loading device in which the FSU (a) was loaded during micro-CT scanning. Force was monitored by a load cell (b), and displacement by an LVDT (c). A bearing (d) ensured that the loading screw (e) did not apply a torque to the specimen

encompassed the entire FSU, from which vertebral body deformations were obtained. Prior to the second scan the target load was reapplied to the FSU, without any preconditioning. Only the endplates were imaged during the second scan, which limited the amount of stress relaxation that occurred in the intervertebral disc and ensured that loads were not redistributed from the nucleus pulposus to the annulus fibrosus [34, 50]. The deflection of the endplate was determined from the second scan. The total deformation of the endplate was defined as the sum of endplate deflection and vertebral body deformation. The loading protocol was repeated on day 2 after 14 h of rehydration within a saline bath with no applied compressive load, allowing the disc to recover height and mechanical properties [22].

Cement augmentation

Specimens were randomly divided into two groups. The third “fractured” group was formed as a result of spontaneous vertebral fracture occurring during testing on day 1. Thus, eight FSUs were assigned to the control group (one T9–T10, one T11–T12, one L1–L2, two L2–L3, three L3–L4), nine FSU fractured and were augmented (three T11–T12, one T12–L1, two L1–L2, one L2–L3, one L3–L4, one L4–L5), and nine were prophylactically augmented (three T12–L1, four L1–L2, one L2–L3, one L4–L5).

Bilateral cement augmentation was performed on vertebrae from the fractured and prophylactic group after testing on day 1, using standard vertebroplasty technique [9, 12, 39] (Fig. 1). Low barium sulfate PMMA cement (Vertecem, Synthes, Switzerland) was injected into the caudal vertebra through 10 gauge cannulae using a custom motorized and instrumented cement injection device [31]. Cement volume was monitored to ensure equal cement distribution. Cement fill volume was standardized to 20% of the vertebral volume. Vertebral volume was estimated based on Vernier caliper measurements, modeling the upper and lower halves of the vertebra as elliptical frusta. Vertebral volume was later verified using the micro-CT scans.

Micro-CT scanning and bone volume compared with total vertebral volume (BV/TV) determination

All measurements were performed on a micro-CT system (XtremeCT, Scanco Medical AG, Bassersdorf, Switzerland). Stack size, to determine endplate deformation, was between 770 and 990 slices with a voxel resolution of 82 μm (field of view 125 mm, $1,536 \times 1,536$ pixels, integration time 399 ms). Total scan time per specimen approached 60 min, for scans of an entire FSU, and 8–16 min for the endplates alone.

Bone volume compared with the total vertebral volume (BV/TV) was determined from micro-CT scans performed in air, using a technique we have previously described [18]. Regional measures of BV/TV have been shown to have a better correlation with vertebral fracture strength than traditional BMD assessment [18]. All parameters for scanning remained equivalent to those described above, except the integration time could be reduced to 200 ms, reducing the scan time for the entire specimen to less than 30 min. BV/TV was determined for ten regions of cancellous bone distal to the cranial endplate and proximal to the caudal endplate (anterior–posterior, superior–inferior, left–right and central). BV/TV was determined using Image Process Language v4.29d (Scanco Medical AG, Bassersdorf, Switzerland).

Determination of endplate deformation

The transformed images of the endplate region of interest (ROI) were segmented by Gaussian filtering (sigma 1.2, support 1) and thresholded (4.75% of maximum gray value) to extract the mineralized phase of the endplate and underlying trabecular bone. Endplate deflection was determined by measuring the relative difference in position of the surfaces of two aligned images (i.e., 200 and 1,000 N loaded specimens) and results were expressed relative to the baseline image (i.e., 200 N loaded specimen). Interpolation was used to minimize partial volume effects when extracting the precise endplate height from the 3D image data (custom code written in C, Visual Studio 6.0, Microsoft; and Matlab, MathWorks Inc, Natick, MA). The determination of endplate surface height, and hence deflection relative to the baseline image, resulted in a spatial map of deflections that could be represented as scalar values superimposed on the endplate surface at each load (Figs. 5, 7).

The point of maximum deflection was located on each endplate surface for each load step by searching for a local maximum. The search space was confined to a user-defined region on the endplate to avoid any errors caused by inclusion of image artifacts that can occur at the margins of the endplate (semi-automatic Matlab routine, MathWorks

Inc, Natick, MA). The same confined search region was applied consistently to all load steps for each specimen, and the position of the local maximum was tracked to monitor if maximum deflection shifted during the experimental protocol.

Statistics

Differences between endplate deformation before and after cement augmentation and FSU stiffness were explored using repeated measures ANOVA. Increases in endplate deflection with a change in load were investigated using a one way ANOVA and a Neuman–Keuls post hoc test (Statistica 7, StatSoft, Tulsa). A significance value of $P = 0.05$ was defined.

Results

Specifics for each treatment group are given in Table 1. In general, for the native specimens there was an increase in endplate deformation with an increase in axial loading (Fig. 3). The mean of the cranial inferior and caudal superior endplate deformation was 0.038 ± 0.022 and 0.082 ± 0.025 mm for an applied stress of 0.62 ± 0.09 N/mm² (load 919 ± 95 N) and 1.08 ± 0.16 N/mm² (load $1,620 \pm 102$ N), respectively ($n = 17$). There was no difference between the deformation of the cranial and caudal endplates ($n = 17$, $P = 0.94$ and $P = 0.46$ for maximum and minimum load, respectively, endplate deformation at maximum load shown in Fig. 4). The maximum deformation of the endplates was partially dependent upon the quality of the subchondral bone ($n = 17$, $R^2 = 0.34$, $P = 0.017$; Fig. 5). Endplate deformations of the fractured group were not included in the determination of unaugmented endplate behavior since

they fractured before scans were obtained at higher loads. Even at lower loads some excessive endplate deformation was noted within the fracture group.

There was no change in stiffness of the FSU before or after cement augmentation for all groups (Table 1).

Deformation of the control FSU

There was no significant difference noted in endplate deformation between the control specimen on day 1 and day 2, signifying that any changes in endplate deformation were due to a change in vertebral behavior under load and not a result of experimental artifact. The difference between day 1 and day 2 endplate deformation, defined by the RMS error [13], was 0.030 mm, which is the effective precision of the protocol [18], compared with an average deformation of 0.084 ± 0.045 mm and maximum

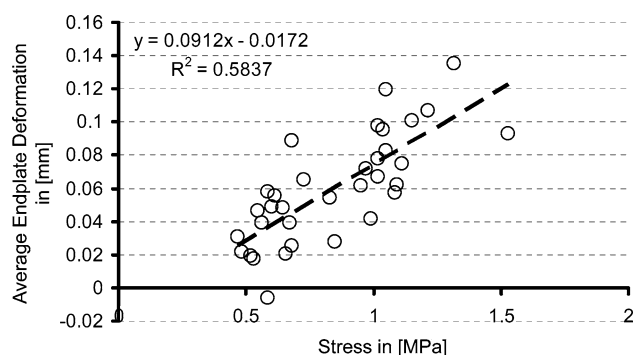


Fig. 3 Average endplate deformation of the cranial inferior and caudal superior endplate for the specimens of the prophylactic and control group prior to cement augmentation. A positive linear correlation was noted between applied compressive stress and endplate deformation ($n = 17$, $P = 0.000$). Each data point represents the mean deformation of the cranial inferior and caudal superior endplate for a FSU at the given load

Table 1 Description of experimental groups

Group	Number of specimen ^a	Age (years \pm SD) ^b	BMD ^c (g/cm ²)	BV/TV ^c (%)	FSU stiffness (N/mm) (days 1 and 2) ^d	Vertebral volume (ml)	Cement volume (% vertebral volume)
Control	8	75.2 \pm 3.93	0.54 \pm 0.4	15.1 \pm 1.8	2,800 \pm 437 2,648 \pm 275 ($P = 0.3$)	40.2 \pm 6.4	NA
Prophylactic	9	76.0 \pm 2.48	0.47 \pm 0.4	13.4 \pm 1.6	2,552 \pm 510 2,567 \pm 442 ($P = 0.7$)	37.1 \pm 5.7	21.9 \pm 3.4
Fractured	5	72.3 \pm 4.77	0.43 \pm 0.4	10.7 \pm 2.4	2,126 \pm 462 2,113 \pm 1,095 ($P = 0.95$)	34.2 \pm 7.6	19.1 \pm 2.5

^a Four specimens (22 of 26 vertebra used, 12 of 13 spines) were excluded from analysis. Two had inadequate cement fill (<15%), one had a cranial inferior endplate failure, and wrong scanning parameters were used for one specimen

^b The age of two specimens was unavailable (2 controls, 2 prophylactic)

^c BV/TV: bone volume compared with the total vertebral volume

^d Stiffness of the FSU was determined when loading the specimen from 1,000 N to its maximum load

^e BMD assessed by anterior–posterior DEXA scans with posterior elements of the vertebrae removed

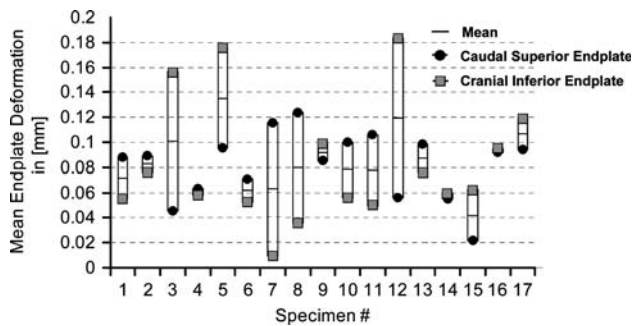


Fig. 4 Interspecimen endplate deformation was heterogeneous. The mean endplate deformation for all specimens was 0.82 ± 0.025 mm at the maximum compressive load applied to the specimen, $1,620 \pm 102$ N. However, endplate deformation was not always equal between the caudal inferior and cranial superior endplate which abut a common disc

deformation of 0.18 mm ($P = 0.41$ maximum load, $P = 0.12$ minimum load, $n = 8$).

Deformation of the adjacent vertebrae

Three FSUs exhibited an increase in adjacent endplate deformation. However, overall the increase in adjacent endplate deformation following cement augmentation of the caudal vertebra was not significant ($P = 0.47$ for maximum load, $n = 9$; Figs. 6, 7). Four of five vertebrae that failed spontaneously during testing on day 1 did not have an increase in adjacent endplate deformation following cement augmentation of the caudal vertebra. One specimen had significant endplate deformation prior to augmentation of the caudal vertebra, possibly sustaining damage to the trabeculae underlying the endplate, hence after cement augmentation of the caudal vertebra, excessive endplate deformation was immediately noted.

Deformation of the augmented vertebrae

Prophylactic cement augmentation of the caudal vertebra resulted in a stiffening of the superior endplate, which was evident in the significant reduction in endplate deformation

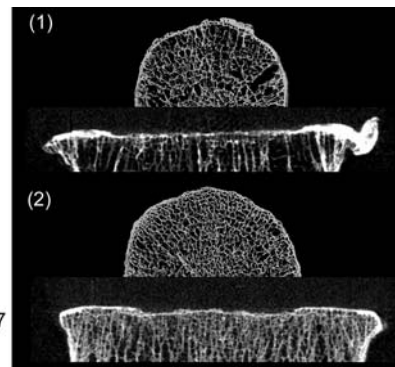
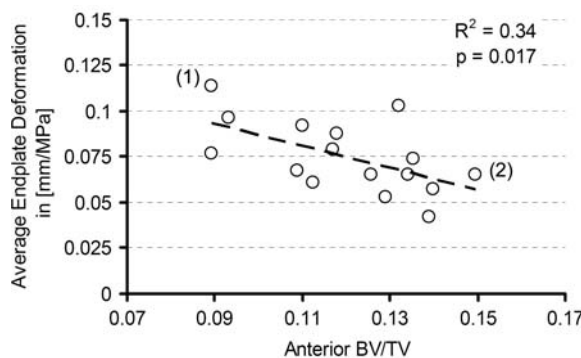
($P = 0.025$, for maximum load, $n = 9$; Fig. 6). However, other regions of the endplate not in direct contact with the cement did deform with magnitudes similar to those observed during unaugmented compression ($P = 0.814$, local maximum, $n = 9$; Fig. 6). Cement augmentation, following fracture of the caudal superior endplate, resulted in significant reinforcement of the endplate and a subsequent reduction in observed endplate deformation ($P = 0.004$, $n = 5$; Figs. 8, 9). Cement must be located directly beneath the endplate for reinforcement to occur; regions that did not have cement in proximity to the endplate were free to deform (Figs. 9, 10).

Discussion

The current repeated measures experimental construct has shown that cement augmentation reduces the endplate deformation of the augmented vertebra and has provided evidence that there was no appreciable alteration in the deformation of the adjacent endplate following cement augmentation. Deformation of the endplates and the vertebral body play an important role in minimizing peak impact loads and reducing strain on intervertebral disc (IVD) annular fibers. Mean endplate deformation was measured to be 0.082 ± 0.25 mm at a load of $1,620 \pm 102$ N, which compares with values found by other investigators [5, 15] ($n = 17$). From the results of Holmes et al., and Brinkmann et al., mean endplate deformations can be interpolated to be 0.106 and 0.153 mm at 1,620 N, respectively. Higher values obtained by previous investigators may be due to the invasive methods used to measure endplate deformation, which disrupts the underlying 3D trabecular structure and likely weakens the vertebrae. However, variation between studies may be also due to inter-specimen variability. We observed a high degree of heterogeneity in endplate response to compressive load between specimens (Fig. 4).

Little evidence was found to support the hypothesis that the adjacent endplate would be subjected to altered loading

Fig. 5 Average cranial inferior and caudal superior endplate deformation correlated with the anterior BV/TV of the underlying subchondral bone (BV/TV: bone volume compared with total vertebral volume). Transverse and coronal sections through the anterior region of specimens with low BV/TV and high endplate deformation (1) and high BV/TV and low endplate deformation (2)



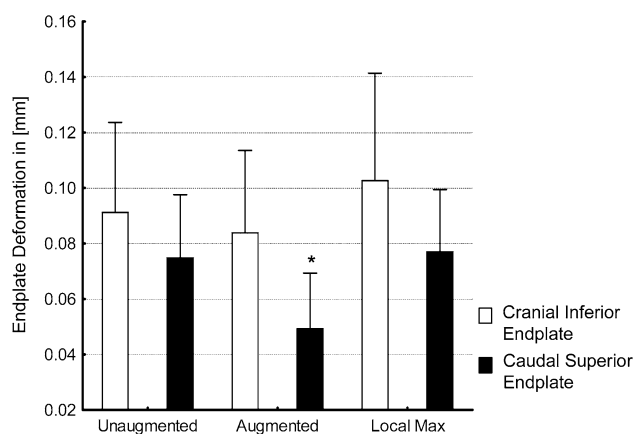


Fig. 6 Deformation of the cranial inferior endplate (adjacent vertebra) and caudal superior endplate (augmented vertebra) for the prophylactic group. No significant change in endplate deformation was noted for the adjacent vertebra after the caudal endplate had been augmented with PMMA (unaugmented – augmented $P = 0.47$, unaugmented – local $P = 0.26$, $n = 9$). A significant reduction in caudal superior endplate deformation was noted following cement augmentation. However, other areas of the endplate not supported by the cement were free to deform as noted by Local Max values. (asterisk, unaugmented–augmented $P = 0.025$, local max–augmented $P = 0.025$, $n = 9$). Data are displayed as the mean endplate deformation at maximum load \pm 95% CI

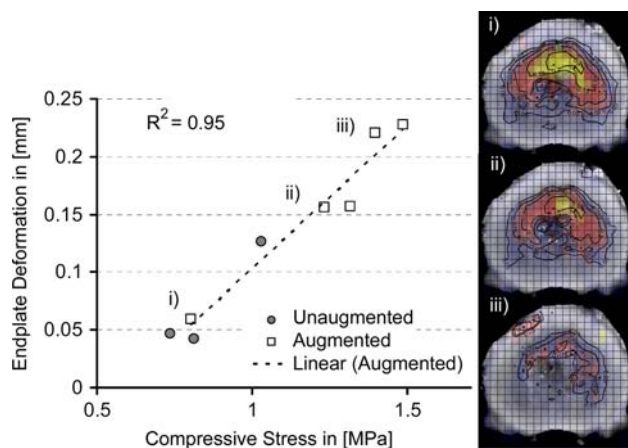


Fig. 7 A typical specimen in which there was no change in cranial inferior endplate (adjacent) deformation pre and post-cement augmentation of the caudal vertebra. Both the unaugmented and augmented endplate deformation lie upon a common linear regression line, indicating no difference between pre and post-cement augmentation endplate behavior (i, ii, iii denote the corresponding deformation map for each loading state shown on the graph; regions with an endplate deformation from lowest to highest are shaded blue, red, yellow, contours are in mm)

and thus be at risk of fracture following cement augmentation. Previous biomechanical in vitro tests [1, 3, 23] and finite element analyses [2, 24, 32, 40, 44, 51] have reported conflicting results. The conflicting results between our experiment and previous finite element analyses may be attributed to differing injection volumes, loading parameters

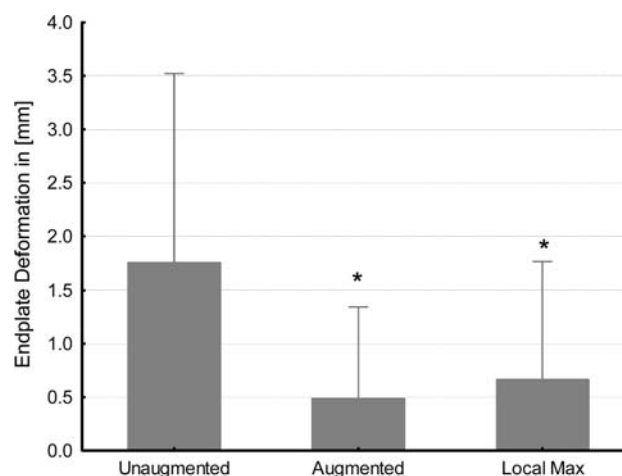


Fig. 8 The caudal superior endplate (augmented) was reinforced following cement augmentation for the fractured group, resulting in a significant reduction in endplate deformation (unaugmented–augmented $P = 0.004$, unaugmented–local maximum $P = 0.004$, $n = 5$). Data are displayed as the mean endplate deformation at maximum load \pm 95% CI

and inability to model the complex behavior of the intervertebral disc and 3D trabecular network. Baroud et al. [2] simulated full filling of the vertebra with cement and only found differences in adjacent endplate deformation using a displacement controlled model; under force control adjacent endplate deformation was only increased by 3%. This is in contrast to the findings of Polikeit et al. [40] and Keller et al. [24], who employed force controlled, partially cement filled models (33–15 and 15%, respectively) and found changes in adjacent endplate deformation. Experimental analysis is equally varied. Berlemann et al., found FSU strength to be 19% lower after intact augmentation, although the experiment was performed with matched specimens, there was no control for vertebral size or disc health, two factors which will influence fracture strength [17]. Kayanja et al. [23], using multi-segmental cadaveric specimens, concluded that adjacent vertebral mechanics were not significantly altered following cement augmentation. However, while the etiology of adjacent vertebral fractures is still in question, this study and previous investigations concur that there are changes in loading (possible stress shielding of the trabeculae around the injected cement) of the augmented vertebra [2, 24]. While this may not be of immediate concern, bone remodeling effects, due to changes in trabecular loading, must be considered when evaluating long-term outcomes.

There are a number of factors that may explain the prevalence of new fractures adjacent to a previously augmented vertebra, including: the distribution and amount of the cement fill, degree of osteoporosis, spinal malalignment, increased patient physical function following surgery [11, 30, 35], and intervertebral disc health. Endplate

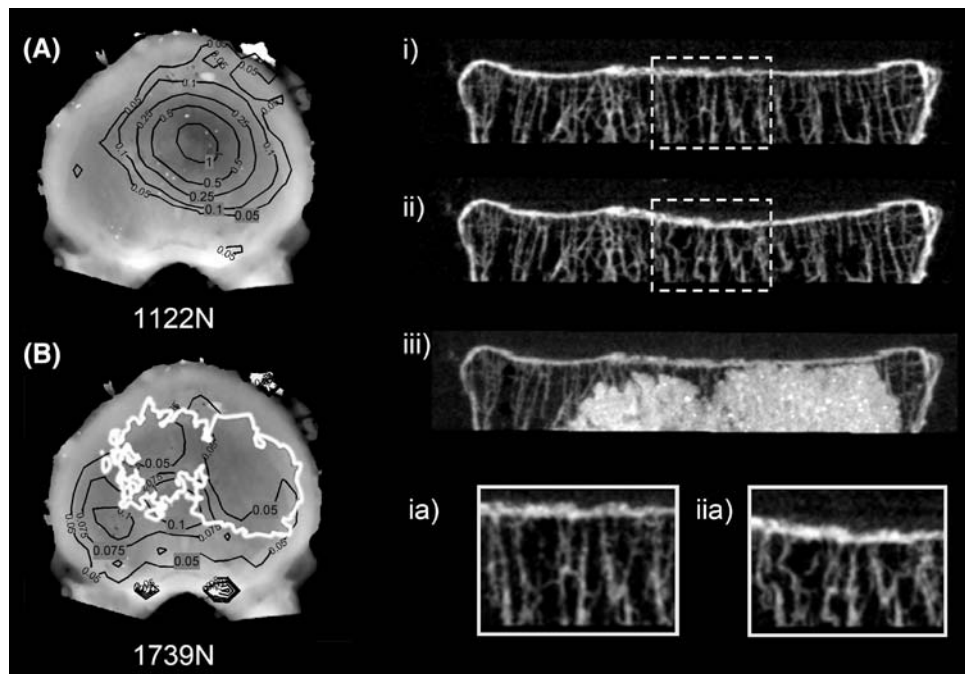


Fig. 9 **a** Deformation map of the caudal superior endplate. Contours show regions of similar deformation. Deformation of the endplate exceeded 1 mm. **b** Endplate deformation map after cement augmentation. *White overlay line* is the boundary of the cement cloud which is in close proximity to the endplate. Within the cement cloud endplate deformation is minimal, however, in regions in which the

cement is not present the endplate is free to deform. *i* Cross section through the region of maximum endplate deformation, 963 N. *ii* Failure of the endplate, 1,800 N. *iii* Stabilization of the endplate after augmentation, 1,739 N. *ia* Detail of the trabecular region (*i*) before any significant endplate deformation, *iia* detail of the trabecular region (*ii*) showing the buckling of the individual trabeculae

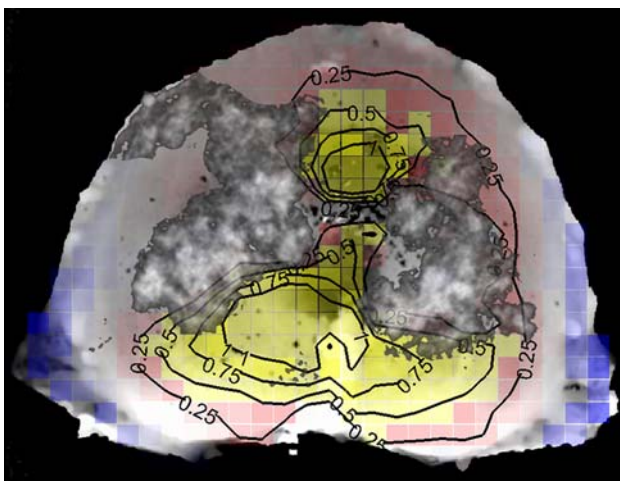


Fig. 10 The endplate was free to deform in regions in which the cement was not directly beneath the endplate. Regions with an endplate deformation from lowest to highest are shaded blue, red, yellow. Contours are in mm

deformation was observed in areas in which the cement was not in close proximity to the endplate (Fig. 8). Heterogeneous cement distribution beneath the endplate, in which one region is supported and another is not, may result in a change in spinal mechanics. Keller et al. [24],

and Lu et al. [32], have noted differences in adjacent endplate stresses with changes in cement fill patterns. Endplate mechanics may also be affected by cement leakage into the disc space, which may also promote adjacent fractures [26, 29, 32].

The strength and stiffness of augmented vertebrae is influenced by the degree of cement fill which may in turn affect the loading of the adjacent vertebra [37]. In studies in which maximum cement fill was achieved, increases in adjacent endplate strains or reductions in FSU strength following cement augmentation are reported [2, 3]. A complete cement fill has additional concerns, including increasing the risks of cement embolism, fat embolism, and cement leakage into the surrounding tissue, resulting in possible neurological complications [19]. Curiously, Keller et al. [24] reported that complete cement fill reduces alterations in intervertebral disc stresses and adjacent segment bone stresses over partial fill. Heterogeneous cement fill patterns may therefore have a greater effect on altered adjacent endplate loading than the stiffness of the cement. The conclusions of this study are based on a cement fill equivalent to 20% of the vertebral volume (approximately 6–8 ml for a typical lumbar vertebra). This value is comparable to that performed clinically (3.9–8.7 ml) [14, 19, 25] and the minimum value required to reduce the fracture risk of high fracture risk vertebral bodies [46].

Rohlmann et al. [44] have proposed that vertebral fracture geometry increases adjacent endplate stresses significantly more than increasing the stiffness of the augmented vertebra through the injection of PMMA. Vertebral collapse is often associated with wedging of the vertebrae [36, 52]. Wedge fractures and resulting kyphosis shift the center of gravity of the upper body, increasing intradiscal pressure and endplate stresses [44]. If the vertebral height is not restored during cement augmentation using patient positioning or mechanical means, the fractured geometry is maintained. We used a simplified loading protocol which considered only compressive loading and did not consider the effect of vertebral geometry on adjacent endplate deformation. Instead, we minimized confounding factors by keeping vertebral geometry constant throughout testing. Vertebral geometry may also change after cement augmentation due to subsidence or uneven endplate deformation as a result of cement placement. Using finite element analysis, Liebschner et al. [28] reported that asymmetric distribution of cement would result in medial–lateral bending motion toward the untreated side. We observed similar endplate behavior. Regions of the endplate which were not directly supported by the injected cement were free to deform (Fig. 10). Thus, asymmetrical cement placement beneath the endplate may result in one region of the endplate being reinforced while another may deform or subside, resulting in changes in spinal alignment and altered loading of adjacent vertebrae.

The effect of cement augmentation is further complicated by disc mechanics. In the current experimental series, loading magnitude was limited to that which may occur during normal daily activities *in vivo*. The importance of endplate deformation is not necessarily realized at low loads. At low loads, the compliance of the FSU is mainly achieved through the medial or sagittal bulging of the IVD. However, at higher loads additional compliance is realized through the deformation of the endplates [4, 5]. Disc health affects the manner in which endplates are loaded. Degenerative discs lack a defined nucleus and under axial compressive loads typically have lower stresses in the anterior half of the disc [41]. Load shift towards the periphery of the vertebral body and the stronger posterior elements decrease the amount of bone at risk of fracture [16, 41]. Since disc health can vary within a spine, studies that do not use a repeated measures design must control for disc health.

There are limitations associated with using this micro-CT based experimental protocol, as well as those associated with all *in vitro* trials. To minimize confounding factors we ensured that our study population was as homogeneous as possible, selecting only elderly specimens. Radiographs in two planes were used to exclude specimens with extensive bony abnormalities or insufficient disc space. While intra-specimen differences do make

generalization of results problematic, perhaps the most important limitation of the current experiment is the time required to perform the scans. Scanning within the micro-CT does not allow analysis of dynamic loading. Loading rate has a significant effect on endplate behavior, due to the viscoelastic properties of the disc [42]. Under quicker loading rates (impact loading), the hydrated disc is essentially incompressible (finite element models often model the nucleus as incompressible), resulting in more reliance on the endplates for compliance, increasing endplate stresses [27]. In this case, a change in stiffness of one of the endplates, due to the presence of cement, may have a greater effect on the adjacent endplate deformation. Measurement resolution of endplate deflection is clearly dependent on the image resolution of the micro-CT (82- μm nominal isotropic resolution). Although measurements below the 82 μm resolution may not be accurate due to resolution limitations, they are reproducible as we have shown with our comparison of deformations on day 1 and day 2 for the control group. Indeed indirect evidence of our ability to measure small endplate deformations was the good correlation observed between native endplate deformation and load. To achieve subvoxel precision, partial volume effects were minimized during image transformation and during endplate surface identification through voxel interpolation of the gray-scale attenuation data [20].

The current study supports the notion that new adjacent fractures may not be a direct result of altered loading due to the presence of the stiff PMMA cement. However, other factors not investigated by this study such as the progression of the osteoporotic disease, dramatic changes in vertebral geometry, heterogeneous cement fill patterns, and indeed application of challenging loads [49] (e.g. impulse loading, forward bending) may result in altered or excessive loading of the adjacent vertebra after cement augmentation, increasing the risk of subsequent vertebral fracture.

Acknowledgments Funding for this research was provided by AOSpine, Dübendorf, Switzerland (Grant # SRN 02/105). The authors wish to thank Josh MacNeil for his assistance with micro-CT data acquisition and analysis, Urs Rohrer, Erland Mülheim and Thomas Gerber for machining the loading device, and Mario Löffel for the use of the cement injection device and associated data acquisition equipment.

References

1. Ananthakrishnan D, Berven S, Deviren V, Cheng K, Lotz JC, Xu Z, Puttlitz CM (2005) The effect on anterior column loading due to different vertebral augmentation techniques. *Clin Biomech* 20:25–31. doi:[10.1016/j.clinbiomech.2004.09.004](https://doi.org/10.1016/j.clinbiomech.2004.09.004)
2. Baroud G, Nemes J, Heini P, Steffen T (2003) Load shift of the intervertebral disc after a vertebroplasty: a finite-element study. *Eur Spine J* 12:421–426. doi:[10.1007/s00586-002-0512-9](https://doi.org/10.1007/s00586-002-0512-9)

3. Berlemann U, Ferguson SJ, Nolte LP, Heini PF (2002) Adjacent vertebral failure after vertebroplasty. A biomechanical investigation. *J Bone Joint Surg Br* 84:748–752. doi:[10.1302/0301-620X.84B5.11841](https://doi.org/10.1302/0301-620X.84B5.11841)
4. Biggemann M, Hilweg D, Brinckmann P (1988) Prediction of the compressive strength of vertebral bodies of the lumbar spine by quantitative computed tomography. *Skelet Radiol* 17:264–269. doi:[10.1007/BF00401809](https://doi.org/10.1007/BF00401809)
5. Brinckmann P, Frobin W, Hierholzer E, Horst M (1983) Deformation of the vertebral end-plate under axial loading of the spine. *Spine* 8:851–856. doi:[10.1097/00007632-198311000-00007](https://doi.org/10.1097/00007632-198311000-00007)
6. Cooper C, Atkinson EJ, Jacobsen SJ, O'Fallon WM, Melton LJIII (1993) Population-based study of survival after osteoporotic fractures. *Am J Epidemiol* 137:1001–1005
7. Cooper C, Atkinson EJ, O'Fallon WM, Melton LJIII (1992) Incidence of clinically diagnosed vertebral fractures: a population-based study in Rochester, Minnesota, 1985–1989. *J Bone Miner Res* 7:221–227
8. Coumans JV, Reinhardt MK, Lieberman IH (2003) Kyphoplasty for vertebral compression fractures: 1-year clinical outcomes from a prospective study. *J Neurosurg* 99:44–50
9. Deramond H, Mathis JM (2002) Vertebroplasty in osteoporosis. *Semin Musculoskelet Radiol* 6:263–268. doi:[10.1055/s-2002-36724](https://doi.org/10.1055/s-2002-36724)
10. Evans AJ, Jensen ME, Kip KE, DeNardo AJ, Lawler GJ, Negin GA, Remley KB, Boutin SM, Dunnagan SA (2003) Vertebral compression fractures: pain reduction and improvement in functional mobility after percutaneous polymethylmethacrylate vertebroplasty retrospective report of 245 cases. *Radiology* 226:366–372. doi:[10.1148/radiol.2262010906](https://doi.org/10.1148/radiol.2262010906)
11. Fribourg D, Tang C, Sra P, Delamarter R, Bae H (2004) Incidence of subsequent vertebral fracture after kyphoplasty. *Spine* 29:2270–2276. doi:[10.1097/01.brs.0000142469.41565.2a](https://doi.org/10.1097/01.brs.0000142469.41565.2a)
12. Gangi A, Guth S, Imbert JP, Marin H, Dietemann JL (2003) Percutaneous vertebroplasty: indications, technique, and results. *Radiographics* 23:e10. doi:[10.1148/rg.e10](https://doi.org/10.1148/rg.e10)
13. Gluer CC, Blake G, Lu Y, Blunt BA, Jergas M, Genant HK (1995) Accurate assessment of precision errors: how to measure the reproducibility of bone densitometry techniques. *Osteoporos Int* 5:262–270. doi:[10.1007/BF01774016](https://doi.org/10.1007/BF01774016)
14. Hodler J, Peck D, Gilula LA (2003) Midterm outcome after vertebroplasty: predictive value of technical and patient-related factors. *Radiology* 227:662–668. doi:[10.1148/radiol.2273011930](https://doi.org/10.1148/radiol.2273011930)
15. Holmes AD, Hukins DW, Freemont AJ (1993) End-plate displacement during compression of lumbar vertebra-disc-vertebra segments and the mechanism of failure. *Spine* 18:128–135. doi:[10.1097/00007632-199301000-00019](https://doi.org/10.1097/00007632-199301000-00019)
16. Homminga J, Weinans H, Gowin W, Felsenberg D, Huiskes R (2001) Osteoporosis changes the amount of vertebral trabecular bone at risk of fracture but not the vertebral load distribution. *Spine* 26:1555–1561. doi:[10.1097/00007632-200107150-00010](https://doi.org/10.1097/00007632-200107150-00010)
17. Hulme PA, Boyd SK, Ferguson SJ (2007) Regional variation in vertebral bone morphology and its contribution to vertebral fracture strength. *Bone* 41:947–957. doi:[10.1016/j.bone.2007.08.019](https://doi.org/10.1016/j.bone.2007.08.019)
18. Hulme PA, Ferguson SJ, Boyd SK (2008) Determination of vertebral endplate deformation under load using micro-computed tomography. *J Biomech* 41:78–85. doi:[10.1016/j.jbiomech.2007.07.018](https://doi.org/10.1016/j.jbiomech.2007.07.018)
19. Hulme PA, Krebs J, Ferguson SJ, Berlemann U (2006) Vertebroplasty and kyphoplasty: a systematic review of 69 clinical studies. *Spine* 31:1983–2001. doi:[10.1097/01.brs.0000229254.89952.6b](https://doi.org/10.1097/01.brs.0000229254.89952.6b)
20. Hwang SN, Wehrli FW (2002) Subvoxel processing: a method for reducing partial volume blurring with application to in vivo MR images of trabecular bone. *Magn Reson Med* 47:948–957. doi:[10.1002/mrm.10138](https://doi.org/10.1002/mrm.10138)
21. Iqbal MM (2000) Osteoporosis: epidemiology, diagnosis, and treatment. *South Med J* 93:2–18
22. Johannessen W, Vresilovic EJ, Wright AC, Elliott DM (2004) Intervertebral disc mechanics are restored following cyclic loading and unloaded recovery. *Ann Biomed Eng* 32:70–76. doi:[10.1023/B:ABME.0000007792.19071.8c](https://doi.org/10.1023/B:ABME.0000007792.19071.8c)
23. Kayanja MM, Evans K, Milks R, Lieberman IH (2006) Adjacent level load transfer following vertebral augmentation in the cadaveric spine. *Spine* 31:E790–E797. doi:[10.1097/01.brs.0000238690.09903.4c](https://doi.org/10.1097/01.brs.0000238690.09903.4c)
24. Keller TS, Kosmopoulos V, Lieberman IH (2005) Vertebroplasty and kyphoplasty affect vertebral motion segment stiffness and stress distributions: a microstructural finite-element study. *Spine* 30:1258–1265. doi:[10.1097/01.brs.0000163882.27413.01](https://doi.org/10.1097/01.brs.0000163882.27413.01)
25. Kobayashi K, Shimoyama K, Nakamura K, Murata K (2005) Percutaneous vertebroplasty immediately relieves pain of osteoporotic vertebral compression fractures and prevents prolonged immobilization of patients. *Eur Radiol* 15:360–367. doi:[10.1007/s00330-004-2549-0](https://doi.org/10.1007/s00330-004-2549-0)
26. Komemushi A, Tanigawa N, Kariya S, Kojima H, Shomura Y, Komemushi S, Sawada S (2006) Percutaneous vertebroplasty for osteoporotic compression fracture: multivariate study of predictors of new vertebral body fracture. *Cardiovasc Intervent Radiol* 29:580–585. doi:[10.1007/s00270-005-0138-5](https://doi.org/10.1007/s00270-005-0138-5)
27. Lee CK, Kim YE, Lee CS, Hong YM, Jung JM, Goel VK (2000) Impact response of the intervertebral disc in a finite-element model. *Spine* 25:2431–2439. doi:[10.1097/00007632-200010010-00003](https://doi.org/10.1097/00007632-200010010-00003)
28. Liebschner MA, Rosenberg WS, Keaveny TM (2001) Effects of bone cement volume and distribution on vertebral stiffness after vertebroplasty. *Spine* 26:1547–1554. doi:[10.1097/00007632-200107150-00009](https://doi.org/10.1097/00007632-200107150-00009)
29. Lin EP, Ekholm S, Hiwatashi A, Westesson PL (2004) Vertebroplasty: cement leakage into the disc increases the risk of new fracture of adjacent vertebral body. *AJNR Am J Neuroradiol* 25:175–180
30. Lindsay R, Silverman SL, Cooper C, Hanley DA, Barton I, Broy SB, Licata A, Benhamou L, Geusens P, Flowers K, Stracke H, Seeman E (2001) Risk of new vertebral fracture in the year following a fracture. *JAMA* 285:320–323. doi:[10.1001/jama.285.3.320](https://doi.org/10.1001/jama.285.3.320)
31. Loeffel M, Heini P, Bouduban N, Burger J, Nolte LP, Kowal J (2007) Development of a computer assisted high pressure injection device for vertebroplasty. *IEEE Trans Biomed Eng* 54:2051–2056. doi:[10.1109/TBME.2007.894964](https://doi.org/10.1109/TBME.2007.894964)
32. Lu S, Xu YQ, Zhang MC, Tang X, Wang YL, Zhong SZ (2007) Biomechanical effect of vertebroplasty on the adjacent intervertebral levels using a three-dimensional finite element analysis. *Chin J Traumatol* 10:120–124
33. Lyles KW, Gold DT, Shipp KM, Pieper CF, Martinez S, Mulhausen PL (1993) Association of osteoporotic vertebral compression fractures with impaired functional status. *Am J Med* 94:595–601. doi:[10.1016/0002-9343\(93\)90210-G](https://doi.org/10.1016/0002-9343(93)90210-G)
34. McMillan DW, Garbutt G, Adams MA (1996) Effect of sustained loading on the water content of intervertebral discs: implications for disc metabolism. *Ann Rheum Dis* 55:880–887. doi:[10.1136/ard.55.12.880](https://doi.org/10.1136/ard.55.12.880)
35. Melton LJIII, Atkinson EJ, Cooper C, O'Fallon WM, Riggs BL (1999) Vertebral fractures predict subsequent fractures. *Osteoporos Int* 10:214–221. doi:[10.1007/s001980050218](https://doi.org/10.1007/s001980050218)
36. Melton LJIII, Kan SH, Frye MA, Wahner HW, O'Fallon WM, Riggs BL (1989) Epidemiology of vertebral fractures in women. *Am J Epidemiol* 129:1000–1011
37. Molloy S, Mathis JM, Belkoff SM (2003) The effect of vertebral body percentage fill on mechanical behavior during percutaneous vertebroplasty. *Spine* 28:1549–1554. doi:[10.1097/00007632-200307150-00014](https://doi.org/10.1097/00007632-200307150-00014)

38. Nachemson AL (1981) Disc pressure measurements. *Spine* 6:93–97. doi:[10.1097/00007632-198101000-00020](https://doi.org/10.1097/00007632-198101000-00020)
39. Peh WC, Gilula LA (2003) Percutaneous vertebroplasty: indications, contraindications, and technique. *Br J Radiol* 76:69–75. doi:[10.1259/bjr/10254271](https://doi.org/10.1259/bjr/10254271)
40. Polikeit A, Nolte LP, Ferguson SJ (2003) The effect of cement augmentation on the load transfer in an osteoporotic functional spinal unit—finite-element analysis. *Spine* 28:991–996. doi:[10.1097/00007632-200305150-00006](https://doi.org/10.1097/00007632-200305150-00006)
41. Pollintine P, Dolan P, Tobias JH, Adams MA (2004) Intervertebral disc degeneration can lead to “stress-shielding” of the anterior vertebral body: a cause of osteoporotic vertebral fracture? *Spine* 29:774–782. doi:[10.1097/01.BRS.0000119401.23006.D2](https://doi.org/10.1097/01.BRS.0000119401.23006.D2)
42. Race A, Broom ND, Robertson P (2000) Effect of loading rate and hydration on the mechanical properties of the disc. *Spine* 25:662–669. doi:[10.1097/00007632-200003150-00003](https://doi.org/10.1097/00007632-200003150-00003)
43. Riggs BL, Melton LJIII (1995) The worldwide problem of osteoporosis: insights afforded by epidemiology. *Bone* 17:505S–511S. doi:[10.1016/8756-3282\(95\)00258-4](https://doi.org/10.1016/8756-3282(95)00258-4)
44. Rohlmann A, Zander T, Bergmann G (2006) Spinal loads after osteoporotic vertebral fractures treated by vertebroplasty or kyphoplasty. *Eur Spine J* 15:1255–1264. doi:[10.1007/s00586-005-0018-3](https://doi.org/10.1007/s00586-005-0018-3)
45. Silverman SL (1992) The clinical consequences of vertebral compression fracture. *Bone* 13(Suppl 2):S27–S31. doi:[10.1016/8756-3282\(92\)90193-Z](https://doi.org/10.1016/8756-3282(92)90193-Z)
46. Sun K, Liebschner MA (2004) Biomechanics of prophylactic vertebral reinforcement. *Spine* 29:1428–1435. doi:[10.1097/01.BRS.0000128760.94173.90](https://doi.org/10.1097/01.BRS.0000128760.94173.90)
47. Trout AT, Kallmes DF, Kaufmann TJ (2006) New fractures after vertebroplasty: adjacent fractures occur significantly sooner. *AJNR Am J Neuroradiol* 27:217–223
48. Truumees E, Hilibrand A, Vaccaro AR (2004) Percutaneous vertebral augmentation. *Spine J* 4:218–229. doi:[10.1016/j.spinee.2003.08.029](https://doi.org/10.1016/j.spinee.2003.08.029)
49. Uppin AA, Hirsch JA, Centenera LV, Pfeifer BA, Pazianos AG, Choi IS (2003) Occurrence of new vertebral body fracture after percutaneous vertebroplasty in patients with osteoporosis. *Radiology* 226:119–124. doi:[10.1148/radiol.2261011911](https://doi.org/10.1148/radiol.2261011911)
50. van Dieen JH, Kingma I, Meijer R, Hansel L, Huiskes R (2001) Stress distribution changes in bovine vertebrae just below the endplate after sustained loading. *Clin Biomech* 16(Suppl 1):S135–S142. doi:[10.1016/S0268-0033\(00\)00105-4](https://doi.org/10.1016/S0268-0033(00)00105-4)
51. Villarraga ML, Bellezza AJ, Harrigan TP, Crompton PA, Kurtz SM, Edidin AA (2005) The biomechanical effects of kyphoplasty on treated and adjacent nontreated vertebral bodies. *J Spinal Disord Tech* 18:84–91. doi:[10.1097/01.bsd.0000138694.56012.ce](https://doi.org/10.1097/01.bsd.0000138694.56012.ce)
52. Wasnich RD (1996) Vertebral fracture epidemiology. *Bone* 18:179S–183S. doi:[10.1016/8756-3282\(95\)00499-8](https://doi.org/10.1016/8756-3282(95)00499-8)
53. Wilcox RK (2004) The biomechanics of vertebroplasty: a review. *Proc Inst Mech Eng* 218:1–10. doi:[10.1243/095441104322807703](https://doi.org/10.1243/095441104322807703)
54. Zoarski GH, Snow P, Olan WJ, Stallmeyer MJ, Dick BW, Hebel JR, De Deyne M (2002) Percutaneous vertebroplasty for osteoporotic compression fractures: quantitative prospective evaluation of long-term outcomes. *J Vasc Interv Radiol* 13:139–148. doi:[10.1016/S1051-0443\(07\)61930-7](https://doi.org/10.1016/S1051-0443(07)61930-7)